Iranian Journal of Analytical Chemistry
Volume 8, Issue 2, September 2021 (15-24) Origonal Research Article

مجله ایرانی شیمی تجزیه
دوره۸، شماره ۲، مهرماه ۱۴۰۰ (۲۴-۱۵)

Electrochemical Behavior of Benzoxanthene Compound in Modified Glassy Carbon Electrode by Zinc Sulfide Particles Warped in CNT/RGO Nanosheets for Determination of Hydrazine

Mohammad Mazloum-Ardakani*, Fatemeh Jokar, Hamideh Mohammadian-Sarcheshmeh, Bi Bi Fatemeh Mirjalili, Sahar Saadat Hosseinikhah
Department of Chemistry, Faculty of Science, Yazd University, 89195-741, Yazd, Iran
Received: 25 August 2021 **Accepted:** 23 September 2021
DOI: 10.30473/ijac.2021.60559.1208

Abstract
Recently, different significant efforts have been made to fabricate an effectively modified electrode for replying to the growing requests for enhanced performance electrodes for electrochemical sensors. Herein, we introduced an organic material along with a composite of the zinc sulfide (ZnS) particles distributed in the substrate of carbon nanotubes (CNTs)/reduced graphene oxide (RGO) nanosheets by using an inexpensive, simple, and one-step fabrication method, as an effectively modified electrode for the determination of hydrazine as an analyte. This electrode represents a great electrochemical performance with a large linear range (0.01 μM-60.0 μM) and a proper limit of detection value (0.006 μM) for determination of hydrazine. Good recovery percentage values for the proposed sensor confirm its excellent ability to measure hydrazine.

Keywords
Zinc Sulfide; Reduced Graphene Oxide; Electrochemical Sensor; Hydrazine.

1. INTRODUCTION

Hydrazine as a flammable liquid has shown an extensive area of applications in fuel-cell, corrosion inhibitor, and reducing reagents. Hydrazine and its derivative also utilize as pesticides in the agriculture and pharmaceutical fields [1]. Despite its many applications, it is toxic in nature, and exposure to it leads to blindness, dizziness and irritation of the nose, eyes, and throat [2, 3]. Hydrazine was classified as group B2 human carcinogens by the World Health Organization (WHO) [4]. So far, various techniques, for example potentiometric [5], fluorometric [6], chromatography [7] and electrochemical techniques have been introduced to determine hydrazine. Among all the applied techniques, the electroanalytical technique is a simple and low-cost procedure with high sensitivity, and reproducibility [8]. Nevertheless, the electrochemical hydrazine oxidation at a bare electrode has slow kinetics and shows very large overpotential, which results in an inappropriate sensing performance [9]. Different kinds of materials such as polymers [10], metal oxide NPs [11], metal NPs [12], metal sulfides [13], and carbon-based material [14-16] have been introduced for modification of bare electrodes to improve the electrochemical behavior of sensors. Among different reported materials, ZnS is widely utilized in the field of electronics and biocatalysis due to its great biocompatibility, good chemical stability, and suitable catalytic performance [17].

Graphene and CNTs have been known as famous materials which are widely utilized in the field of electrochemical studies. Graphene is a 2D nanostructure with an excellent specific surface area, and great conductivity [18]. Newly, RGOs and their various nanocomposites have been extensively introduced in the fabrication of sensors to enhance electrochemical functions [19-21]. Carbon nanotubes have acquired a lot of attention in different fields of material science and technologies because of their outstanding properties involving high conductivity [22] large surface area and having electrocatalytic behavior [23, 24]. Herein, a modified glassy carbon electrode (GCE) was introduced by using a benzoxanthenederivative, 12-(3,4-dihydroxyphenyl)-9,9-dimethyl-8,9,10,12 tetrahydrobenzo[a]xanthen-11-one (DX), and a composite of ZnS particles distributed in the substrate of CNTs/RGO nanosheets combination (ZW) to study the electrochemical performance of hydrazine. The composite of ZW was fabricated by an inexpensive, facile, and one-step hydrothermal method. After fabrication of DX and ZW, some characterizations were done and finally, electrochemical behavior of the analyte was examined by modified GCE (ZW/DX/GCE) in different electrochemical studies involving cyclic

*Corresponding Author: mazloum@Yazd.ac.ir

voltammetry (CV) and differential pulse voltammetry (DPV).

2. EXPERIMENTAL

2.1. Apparatus and materials

Electrochemical examinations were carried out by using a potentiostat galvanostat impedance analyzer, model Radstat 1A (IRAN). A three-electrode cell was utilized. Ag/AgCl/KCl (3.0 M) electrode, a platinum wire, and the modified GCE (DX/ZW/GCE) were respectively applied as the reference, counter, and working electrodes. The CNT was bought from Plasma Chem and other materials were from analytical class (Merck, Germany).

2.2. Synthesize of 12-(3,4-dihydroxyphenyl)-9,9-dimethyl-8,9,10,12-tetrahydrobenzo[a]xanthen-11-one or (DX)

1 mmol of 2-naphthol, 1 mmol of 3,4-dihydroxybenzaldehyde, 1 mmol of dimedone, and 0.030 g of Fe_3O_4@nano-cellulose/Sb(V) was mixed at 80 °C. After completion of the reaction (checked by TLC, n-hexane: EtOAc (1:1)), the mixture was dissolved in ethanol and the catalyst was separated using an external magnet. By adding water to remained mixture, the DX was obtained as a pure solid. Scheme 1 shows the structure of DX.

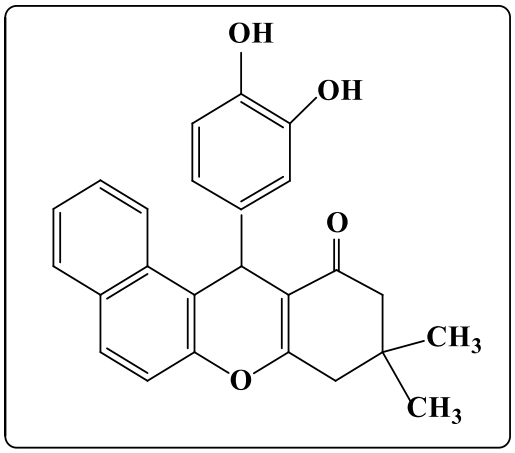

Scheme 1. Structure of 12-(3,4-dihydroxyphenyl)-9,9-dimethyl-8,9,10,12-tetrahydrobenzo[*a*] xanthen-11-one or (DX).

2.3. Synthesize of a composite of ZnS particles distributed on the CNTs/RGO nanosheets (ZW)

Firstly, GO was synthesized by the improved Hummers method [25]. Then, the ZW composite was fabricated by using $Zn(NO_3)_2 \cdot 6H_2O$ according to previously reported work [26].

2.4. Electrode preparation

The GCE was polished by using the alumina powder, washed and dried in the environmental condition. First, 8.0 mg of the composite was dispersed in the ethanol. 2.5 µL of the solution was cast on the GCE and dried at environmental to get ZW/GCE. Then, 2.5 µL of DX solution (5.0 mM) was cast on the ZW/GCE and then dried to provide a modified electrode of DX/ZW/GCE.

2.5. Preparation of solutions

To prepare phosphate buffer with different pHs, 0.1 M solution of phosphoric acid was prepared by distilling water and the desired pH was adjusted by NaOH solution. To prepare hydrazine and hydroxylamine solutions, the suitable amount of materials were dissolved in phosphate buffer 0.1 M (pH = 9.0).

3. RESULT AND DISCUSSION

3.1. Characterization

The structure of DX has been studied by Fourier transform spectroscopy (FTIR) and nuclear magnetic resonance (NMR). ***FTIR (ATR)***, $\bar{\upsilon}$, cm^{-1}: 3468, 2969, 1613, 1591, 1378, 1222, 806, 751. (Fig. 1). ***^{1}H NMR*** (500 MHz, $CDCl_3$)/ δ(ppm): 0.98 (s, 3H), 1.11 (s, 3H), 2.23 (d, 1H, *J* = 6 Hz), 2.46 (s, 1H), 2.57 (s, 1H), 5.62 (s, 1H), 6.56 (dd, 3H, *J* = 21, 8.5 Hz), 7.07 (s, 1H), 7.31 (d, 1H, *J* = 9 Hz), 7.31-7.42 (m, 1H), 7.78 (t, 2H, *J* = 9 Hz), 8.00 (d, 1H, *J* = 8.5 Hz) (Fig. 2). ***^{13}C NMR*** (125 MHz, $CDCl_3$)/δ ppm: 25.21, 27.20, 29.27, 32.57, 37.92, 38.89. 54.89, 83.39, 86.30, 95.41, 99.50, 108.08, 114.60, 115.72, 117.88, 131.70, 137.36, 142.66, 143.72, 147.73, 153.03, 154.33, 158.89, 165.14, 199.03 (Fig. 3).

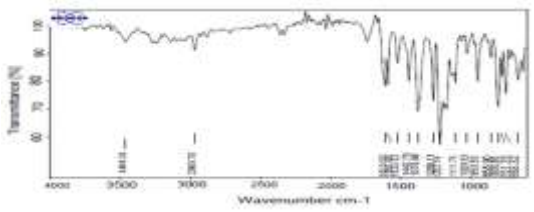

Fig. 1. FT-IR spectrum of DX.

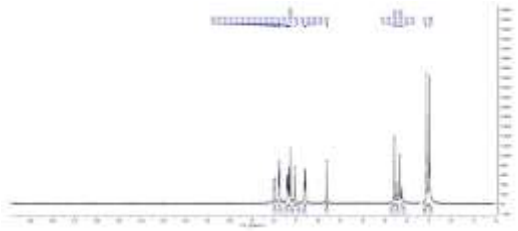

Fig. 2. ^{1}H NMR of DX.

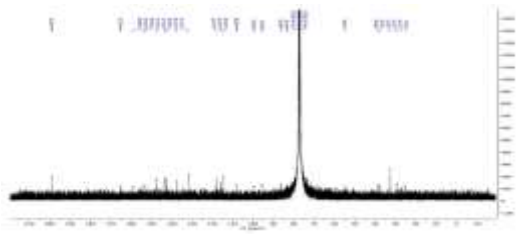

Fig. 3. ^{13}C NMR spectrum of DX.

Fig. 4. Exhibits SEM image of ZW composite. The SEM for ternary nanocomposite, RGO-CNT-ZnS, shows the formation of ZnS particles on RGO sheets, and the proper distribution of CNTs in the matrix. In this structure, the CNTs can operate such as spacers for graphene planes to create ‘‘channels’’ for the transfer of electrons.

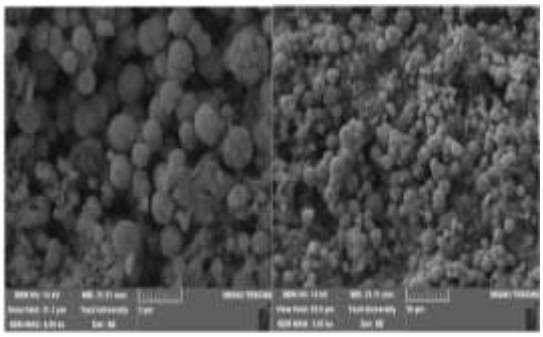

Fig. 4. SEM images for the composite of ZnS particles distributed on the CNTs/RGO nanosheets (ZW)**.**

Fig. 5. Shows XRD pattern for the synthesized composite of ZW. Some relatively intensive peaks almost at 27.08°, 28.56°, 30.62°, 47.64°, and 56.50° are attributed to the crystal of phase ZnS [27]. In addition, there isn't any characteristic peak of GO (at 10 °) for composite, confirming the reduction of GO during the synthesis process. FT-IR spectrum of ZW composite (Fig. 6) shows bands at 615 cm^{-1} and 1097 cm^{-1} which confirm the characteristic peaks of the ZnS material [28, 29]. Peeks at 1720 cm^{-1}, 1265 cm^{-1} and 900 cm^{-1} are assigned to COOH, OH and C-O functional groups reveal the presence of the CNT in the composite [30, 31]. The common characteristic peaks of GO sample are O-H, C=O, C=C, C-OH and C-O stretching vibrations at 3403, 1725, 1628, 1193 and 1046 cm^{-1}, respectively; the O-H bending vibrations of C-OH at 1382 cm^{-1} [32, 33]. These absorption peaks were almost disappeared for the prepared composite, which shows GO changed to RGO during the hydrothermal synthesis method [34].

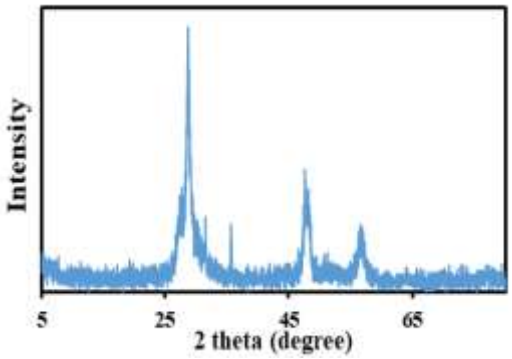

Fig. 5. XRD patterns of ZW.

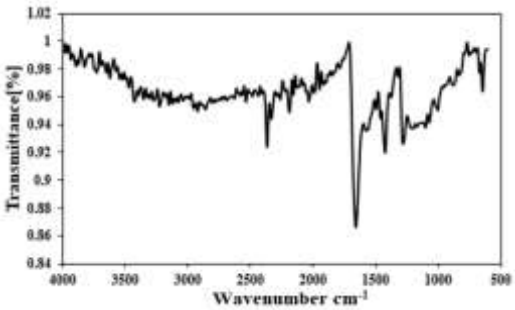

Fig. 6. FTIR spectra of ZW.

3.2. The electrochemical behavior of DX/ZW/GCE

All electrochemical responses of the modified electrode (DX/ZW/GCE) were studied by the CV technique in a phosphate buffer solution (0.10 M) with various pH values (3.0 – 11.0) in Fig. 7. The anodic and cathodic potential peaks (E_{pa}, E_{pc}) were moving toward low potentials with increasing in pH value and a maximum current obtained at pH=9.0. It was selected as the optimized amount. A potential-pH plot (inset of Fig. 7) exhibits a line with a slope value of -56.6 mV/pH, which reveals the same electrons and protons transfer reaction.

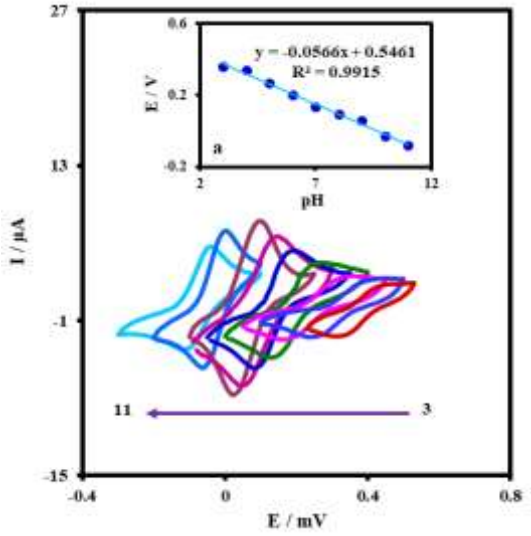

Fig. 7. CVs of DX/ZW/GCE in 0.1 M phosphate buffer solution (pH= 9.0). The pH values from (3) to (11) Scan rate: 100 mV s^{-1}. Inset: Variation of E_p as a function of pH.

In order to investigate the electrochemical behavior of DX/ZW/GCE, cyclic voltammograms were measured at various scan rates in the absence of hydrazine at optimized pH. The voltammograms in Fig. 8 exhibited that the electrochemical process was quasi-reversible due to the ΔE_p value of higher than (59/n) mV. Fig. 8, inset of (a) showed that both peak currents were directly dependent on scan rate in the range of 5 to 900 mV s^{-1}, confirming that the redox process happened in a surface-

limited redox process. The amount of "*Γ*" (surface coverage of modified electrode) was calculated by using the slope of the anodic peak current and Sharp equation [35]. It was $\Gamma = 2.1\times10^{-10}$ mol/cm^2. In order to calculate kinetic parameters of the electron transfer rate constant (k_s) and the transfer coefficient (α) for the modified electrode, the variations of E_{pa} and E_{pc} were plotted versus the logarithm of scan rates (Inset (b) and (c)). At high scan rates, there is a linear section. The slope amount in the linear section is equivalent to $2.3RT/(1-\alpha)n_\alpha F$ for anodic peak and $-2.3RT/\alpha n_\alpha F$ for the cathodic peak [36]. The values of cathodic and anodic transfer coefficients ($\alpha_c = 0.69$ and $\alpha_a = 0.31$) were obtained by using the above equations and slopes. Furthermore, by Laviron procedure [36] obtain $k_s = 4.2$ s^{-1} for the modified electrode.

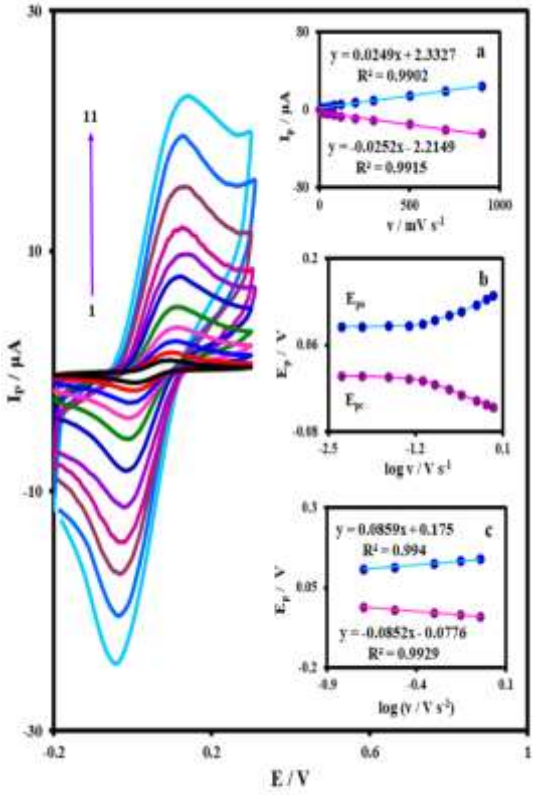

Fig. 8. CVs of DX/ZW/GCE in buffer solution with a pH value of 9.0 at several scan rates, (5.0, 10, 25, 50, 80, 120, 200, 300, 500, 700, and 900 mV s^{-1}), insets: (a) plot of I_p against v, (b) and (c) E_p against log v.

3.3. Electrocatalytic properties of the DX/ZW/GCE electrode for hydrazine

Cyclic voltammetry was recorded at various scan rates in the presence of hydrazine (0.30 mM). Fig. 9 exhibited that the E_{pa} for hydrazine oxidation at the bare GCE was 450 mV (curve b), while the E_{pa} at DX/ZW/GCE is 140 mV (curve f). It exhibits that the E_p of hydrazine oxidation decreases around 310 mV at the modified electrode. However, DX/ZW/GCE (curve f) shows a higher current toward hydrazine compared to DX/GCE (curve e), indicating that the utilization of the ZW composite can increase the peak currents because of its remarkable conductivity and good surface area. The DX/ZW/GCE in a buffer solution (pH=9.0), without hydrazine, represented a redox process (curve d). After using 0.30 mM hydrazine; the anodic peak increased, while the cathodic peak decreased (curve f) for the modified electrode. All these results confirmed that there was an electrocatalytic performance for oxidation of hydrazine at the DX/ZW/GCE by an EC′ mechanism. According to this process, hydrazine is oxidized in a catalytic chemical reaction (C′) by using the oxidized species of DX (DX_{ox}) which is provided by an electrochemical reaction (E). The oxidation reaction is catalyzed for hydrazine and thus anodic current increases.

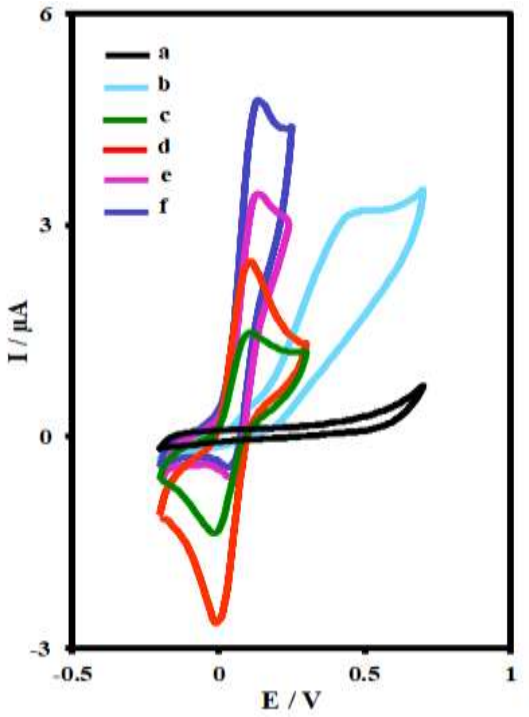

Fig. 9. Cyclic voltammograms of (a) bare GCE in buffer solution (pH=9.0) at v=25 mV s^{-1}; (b) as (a) + 0.30 mM hydrazine; (c) as (a) at DX /GCE; (d) as (a) at DX/ZW/GCE; (e) as (c) + 0.30 mM hydrazine; (f) as (b) at the surface of DX/ZW/GCE.

The electrocatalytic behavior of analyte at various scan rates was exhibited in Fig. 10. A linear dependence between peak current (I_p) and the square root of the scan rate ($\upsilon^{1/2}$) (inset of (a)) implies that the electrochemical process is controlled by diffusion. Therefore, a curve of the scan rate normalized current ($I_p/\upsilon^{1/2}$) against scan rates (inset of (b)) confirms a process with an EC′ mechanism for electrocatalytic oxidation of analyte.

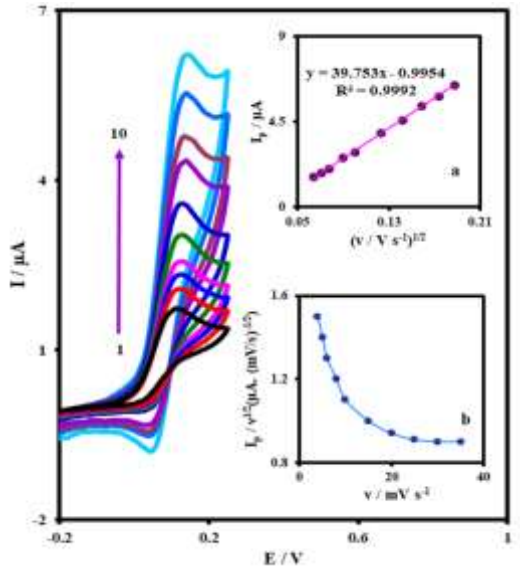

Fig. 10. CV curves of DX/ZW/GCE in the presence of 0.30 mM hydrazine at different scan rates (4.0, 5.0, 6.0, 8.0, 10, 15, 20, 25, 30 and 35 mV s^{-1}), plot of (a) I_{pa} versus $v^{1/2}$ and (b) plot of (I_p /$v^{1/2}$) against v.

The Tafel plot (Fig. 11), plotted by utilization of the obtained data from the rising section of the voltammogram at v=20 mV s^{-1} was applied to calculate the charge transfer coefficient (α=0.38).

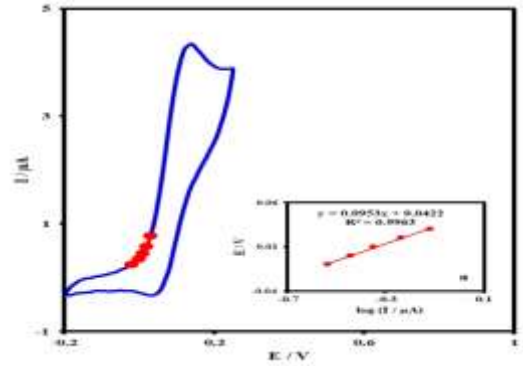

Fig. 11. Illustrated tafel plot by using the ascending part of voltammogram recorded at v=20 mV s^{-1}.

3.4. Chronoamperometric examination

Chronoamperometric investigation of analyte at DX/ZW/GCE was done to estimate the diffusion coefficient (D). The chronoamprograms of DX/ZW/GCE were recorded by placing the modified electrode potentials at +0.20 V vs. Ag/AgCl for hydrazine at different concentration values (Fig. 12). The diffusion coefficient (D) value is obtained by using the Cottrell equation and the slopes of the linear plot of I_p vs. $t^{-1/2}$ (inset of (a) and (b)). The D value was 1.99×10^{-5} cm^2/s [37]. Also, the chronoamperometric technique was applied to obtain the catalytic rate constant of analyte at DX/ZW/GCE by using eq. 1 [38]:

$$I_C/I_L = \gamma^{1/2}[\pi^{1/2}\,\mathrm{erf}(\gamma^{1/2}) + \exp(-\gamma)/\gamma^{1/2}] \quad \text{(Eq. 1)}$$

Where I_C and I_L are the catalytic and limiting currents of DX/ZW/GCE in the absence and presence of the analyte and $\gamma = kC_bt$. Where C_b is the bulk concentration for hydrazine (mol/cm^3). If $\gamma > 2$, the error function is equal to 1 and eq. 1 changes to eq. 2:

$$I_C/I_L = \pi^{1/2}\gamma^{1/2} = \pi^{1/2}(kC_bt)^{1/2} \quad \text{(Eq. 2)}$$

Where t is the time (s). The eq. 2 is used to estimate the rate constant of the catalytic process (k). From the slope of the I_C/I_L versus $t^{1/2}$ plot, k obtains for hydrazine. By using the slopes (the chronoamprograms in Fig. 12, inset (c)), the average value of k is 1.34×10^4 $M^{-1}s^{-1}$.

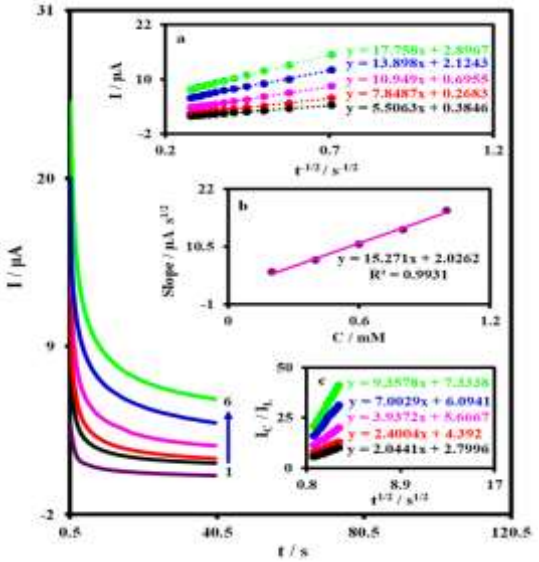

Fig. 12. Chronoamperograms obtained at DX/ZW/GCE in 0.1 M phosphate buffer solution (pH 9.0) for different concentrations of hydrazine. The numbers 1–6 correspond to 0.0, 0.2, 0.4, 0.6, 0.8 and 1.0 mM of hydrazine. Insets: (a) plots of I vs. $t^{-1/2}$ obtained from chronoamprograms, (b) plot of the slope of the straight lines against the hydrazine concentration and (c) plot of I_C/I_L vs. $t^{1/2}$ obtained from chronoamprograms.

3.5. Calibration curve and obtaining limit of detection

In order to achieve calibration equation and estimate the limit of detection (LOD), a sensitive and effective technique is DPV [39]. The DPV responses of the DX/ZW/GCE for hydrazine with different concentrations were shown in Fig. 13. Adjustments in differential pulse voltammetry measurements: E start(V)=-0.04, E end(V)=0.2, Scan rate(V/s)=0.05, Pulse time(s)=0.05, E step(V)=0.01. The calibration equation for hydrazine in the range of 0.01–0.80 µM was I_p (µA) = (10.688) $C_{hydrazine}$ + (5.206) (R^2=0.994), and for hydrazine in the range of 0.80– 60.0 µM was I_p (µA) = (0.1198) $C_{hydrazine}$ + (15.652) (R^2=0.990). The LOD value of 0.006 µM was obtained by

using the slope of the calibration curve in the lower concentration linear range.

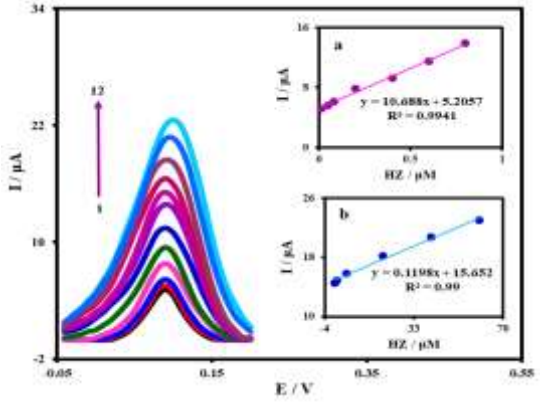

Fig. 13. DPV measurement of DX/ZW/GCE in the buffer solution containing various concentrations of hydrazine. The numbers of 1–12 are corresponding to 0.010, 0.050, 0.080, 0.20, 0.40, 0.60, 0.80, 1.0, 5.0, 20.0, 40.0 and 60.0 µM of hydrazine. Insets show the plots of the electrocatalytic peak current as a function of hydrazine concentration in the range of (a) 0.01-0.80 µM and (b) 0.80-60.0 µM.

3.6. Simultaneous determination of hydrazine and hydroxylamine

The change of oxidation peak currents with the increasing concentration of hydrazine and hydroxylamine were simultaneously examined by using the DPV technique at DX/ZW/GCE. Fig. 14 displays individual oxidation peaks for hydrazine and hydroxylamine with a potential value of -120 and 440 mV. The sensitivity of the DX/ZW/GCE electrode for hydrazine oxidation is 10.69 µA μM^{-1} and for hydrazine oxidation in the presence of hydroxylamine is 10.81 µA μM^{-1}. Our conclusions imply the sensitivities of the DX/ZW/GCE for hydrazine in two conditions are nearly similar. Thus, hydrazine can be measured without any interference.

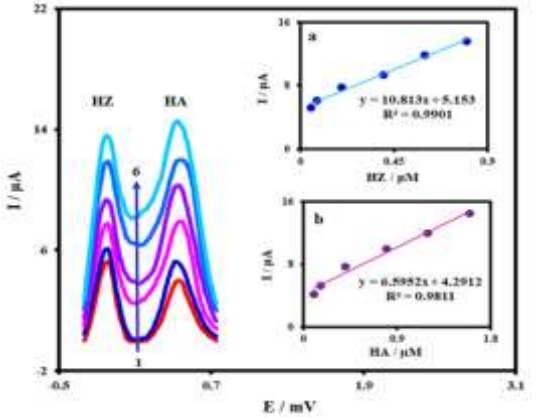

Fig. 14. DPVs of DX/ZW/GCE in buffer solution (pH=9.0) containing different concentrations of HZ and HA: from inner to outer corresponds to mixed solutions of 0.050+0.094, 0.080+0.150, 0.200+0.380, 0.400+ 0.750, 0.600+1.120 and 0.800+1.500, (a) Calibration plot of HZ and (b) Calibration plot of HA

3.7. Measurement of hydrazine in water samples

To study hydrazine in the real sample, drinking water sample in 0.1 M phosphate buffer solution (pH = 9.0) and pulsed voltammetry method was used. To do this, 10.0 mL of the actual sample of drinking water in a balloon was increased to 20.0 mL by phosphate buffer with pH = 0.9 and then to evaluate the performance and accuracy of measuring a certain amount of solution of the sample with concentration. The desired solution was added to the solution and the measurement was performed by differential pulse voltammetry.To estimate the performance of the introduced sensor in the real sample analyses, the hydrazine concentration was determined in the water sample. For the preparation of synthetic samples, specific amounts of hydrazine are added to the drinking water sample. The calculated values were achieved in the Table. 1. The obtained recovery percentages for the samples were 98.0, 98.5, 101, and 99.5%, and the RSD of the parallel tests was less than 1.0%, indicating that the DX/ZW/GCE could be effectively utilized to detect hydrazine in the drinking water.

Table. 1. The application of modified GCE for determination of hydrazine in water sample.

Hydrazine Added (µM)	Found (µM)	Recovery (%)	RSD (%)
0.050	0.049	98.0	3.30
0.600	0.591	98.5	1.00
0.800	0.809	101	1.80
40.0	39.8	99.5	2.40

3.8. The repeatability and reproducible of DX/ZW/GCE

In order to examine the reproducibility of DX/ZW/GCE, DPVs were recorded for 8 separately prepared DX/ZW/GCE for the determination of hydrazine. The RSD value for anodic current peeks was 2.86%, indicating good reproducibility of the modified electrode. Additionally, a repeatability study was examined by recording continuous DPVs for a DX/ZW/GCE after 20 times. The data revealed the RSD amount of 2.48%. These results show that DX/ZW/GCE has good reproducibility and repeatability for the electrochemical determination of hydrazine.

3.9. Interference study

An important parameter to develop sensors is their ability to discriminate between the interfering species. Herein, the DPV technique was used to investigate hydrazine in the presence of interferes. The data were exhibited in Table. 2. The obtained data revealed that the fabricated sensor had a good selectivity.

3.10. Comparison of results

Our results were compared with other similar works (Table. 3). This work shows a larger

concentration range and also the best LOD value. Also, it can be said that the modified electrode in this work is efficient for measuring hydrazine due to the low cost, easy and fast preparation method.

Table. 2. Interference investigation for the determination of analyte in the optimized conditions.

Specie	Tolerante limit $W_{Substance}/W_{Specie}$	Specie	Tolerante limit $W_{Substance}/W_{Specie}$
Cu^{2+}	157	F^-	95
Pb^{2+}	100	Cl^-	176
Co^{2+}	294	SCN^-	290
Ag^+	529	NO_3^-	304
Na^+	115	Citrate	24
Acetate	589	Uric Acid	63

4. CONCLUSION

The present modified electrode by DX/ZW/GCE composite displayed an excellent performance with a good wide linear range to measure hydrazine. The modification of GCE improved sensitivity, selectivity and provide the best capability for simultaneous measurement of hydrazine and hydroxylamine. The proposed composite exhibited significant electron transfer capability in redox-active solution. The CV and DPV investigations showed acceptable electrocatalytic responses of the DX/ZW/GCE in decreasing the anodic overpotential for the hydrazine oxidation. Also, the test results of real samples revealed that the DX/ZW/GCE is reliable to determine analyte in drinking water samples.

Funding

This research did not receive any specific grant from funding agencies in the public, commercial, or not-for-profit sectors.

Conflicts of interest

There is no conflict to declare.

ACKNOWLEDGEMENTS

The authors would like to thank Yazd University Research Council for financial support of this research.

REFERENCES

[1] G. Srinidhi, S. Sudalaimani, K. Giribabu, S. S. Basha and C. Suresh, 2020 Amperometric determination of hydrazine using a CuS-ordered mesoporous carbon electrode, *Microchim. Acta* 187 (2020) 1.

[2] G. Choudhary and H. Hansen, Human health perspective of environmental exposure to hydrazines: A review, *Chemosphere* 37 (1998) 801.

[3] E. Vernot, J. MacEwen, R. Bruner, C. Haun, E. Kinkead, D. Prentice, A. Hall III, R. Schmidt, R. Eason R and G. Hubbard, Long-term inhalation toxicity of hydrazine, *Fundam. Appl. Toxicol.* 5 (1985) 1050.

[4] M. H. Jazayeri, T. Aghaie, A. Avan, A. Vatankhah and M. R. S. Ghaffari, Colorimetric detection based on gold nano particles (GNPs): An easy, fast, inexpensive, low-cost and short time method in detection of analytes (protein, DNA, and ion), *Sens. Bio Sens. Res.* 20 (2018) 1.

[5] J. W. Mo, B. Ogorevc, X. Zhang and B. Pihlar, Cobalt and copper hexacyanoferrate modified carbon fiber microelectrode as an all-solid potentiometric microsensor for hydrazine, *Electroanalysis* 12 (2000) 48.

[6] Y. Hao, Y. Zhang, K. Ruan, W. Chen, B. Zhou, X. Tan, Y. Wang, L. Zhao, G. Zhang and P. Qu, A naphthalimide-based chemodosimetric probe for ratiometric detection of hydrazine, *Sens. Actuator B Chem.* 244 (2017) 417.

Table. 3. Evaluation of analytical results of different works to determinate hydrazine.

Electrode	LOD (μM)	Linear range (μM)	Ref
MnO_2 Nanostructures	2.1	$30\text{-}2.8\times10^{+3}$	40
Cu_xO–PEDOT	0.20	$0.50\text{-}6.0\times10^{+2}$	41
Mesoporous Au/ZnO	0.24	$0.20\text{-}2.0\times10^{+2}$	42
ZnMOF/ETH500/nafion	2.0	$20\text{-}3.5\times10^{+2}$	43
Ag/ZIF-67/CPE	1.4	$4.0\text{-}3.3\times10^{+2}$, $3.3\times10^{+2}\text{-}4.7\times10^{+2}$	44
AuNPs@NPC-rGO	9.6×10^{-2}	0.050-1.0	45
Co_3O_4/MWCNT	0.80	$20\text{-}11\times10^{+2}$	46
TiO_2@PANI@Au NPs	0.15	$0.90\text{-}12\times10^{+2}$	47
APC-CNT	0.0086	0.01-120.0	48
ZW composite	0.006	0.01-0.80, 0.80-60.0	This work

[7] M. Sun, L. Bai and D. Q. Liu, A generic approach for the determination of trace hydrazine in drug substances using in situ derivatization-headspace GC–MS, *J. Pharm. Biomed. Anal.* 49 (2009) 529.

[8] P. Shaikshavali, T. M. Reddy, T. V. Gopal, G. Venkataprasad, V. S. Kotakadi, V. Palakollu and R. Karpoormath, A simple sonochemical assisted synthesis of nanocomposite (ZnO/MWCNTs) for electrochemical sensing of Epinephrine in human serum and pharmaceutical formulation, *Colloid Surf. A: Physicochem. Eng. Asp.* 584 (2020) 124038.

[9] S. Mutyala and J. Mathiyarasu, Preparation of graphene nanoflakes and its application for detection of hydrazine, *Sens. Actuator B Chem.* 210 (2015) 692.

[10] M. Gerard, A. Chaubey and B. Malhotra, Application of conducting polymers to biosensors, *Biosens. Bioelectron.* 17 (2002) 345.

[11] S. Radhakrishnan, K. Krishnamoorthy, C. Sekar, J. Wilson and S. J. Kim, A highly sensitive electrochemical sensor for nitrite detection based on Fe_2O_3 nanoparticles decorated reduced graphene oxide nanosheets, *Appl.Catal. B: Environ.* 148 (2014) 22.

[12] D. Rao, Q. Sheng and J. Zheng, Novel nanocomposite of chitosan-protected platinum nanoparticles immobilized on nickel hydroxide: facile synthesis and application as glucose electrochemical sensor, *J. Chem. Sci.* 128 (2016) 1367.

[13] J. Amani, A. Khoshroo and M. Rahimi-Nasrabadi, Electrochemical immunosensor for the breast cancer marker CA 15–3 based on the catalytic activity of a CuS/reduced graphene oxide nanocomposite towards the electrooxidation of catechol, *Microchim. Acta* 185 (2018) 79.

[14] N. Zou, X. Wei, Z. Zong, X. Li, Z. Wang and X. Wang, A novel enzymatic biosensor for detection of intracellular hydrogen peroxide based on 1-aminopyrene and reduced graphene oxides, *J. Chem. Sci.* 131 (2019) 1.

[15] J. H. Jung, D. S. Cheon, F. Liu, K. B. Lee and T. S. Seo, A graphene oxide based immuno-biosensor for pathogen detection, *Angew. Chem.* 122 (2010) 5844.

[16] J. J. Feminus, R. Manikandan, S. S. Narayanan and P. Deepa, Determination of gallic acid using poly (glutamic acid): graphene modified electrode, *J. Chem. Sci.* 131 (2019) 11.

[17] N. Suganthi and K. Pushpanathan, Paramagnetic nature of Mn doped ZnS nano particles in opto electronic device application, *J. Mater. Sci.: Mater. Electron.* 27 (2016) 10089.

[18] W. Lv, J. Zhao, B. Situ, B. Li, W. Ma, J. Liu, Z. Wu, W. Wang, X. Yan and L. Zheng, A target-triggered dual amplification strategy for sensitive detection of microRNA, *Biosens. Bioelectron.* 83 (2016) 250.

[19] G. Yu, W. Wu, X. Pan, Q. Zhao, X. Wei and Q. Lu, High sensitive and selective sensing of hydrogen peroxide released from pheochromocytoma cells based on Pt-Au bimetallic nanoparticles electrodeposited on reduced graphene sheets, *Sensors* 15 (2015) 2709.

[20] H. Shamkhalichenar and J-W Choi, Review-Non-enzymatic hydrogen peroxide electrochemical sensors based on reduced graphene oxide, *J. Electrochem. Soc*. 167 (2020) 037531.

[21] P. A. Raymundo-Pereira, M. Baccarin, O. N. Oliveira Jr and B. C. Janegitz, Thin films and composites based on graphene for electrochemical detection of biologically-relevant molecules, *Electroanalysis* 30 (2018) 1888.

[22] H. Beitollahi, F. Movahedifar, S. Tajik and S. Jahani, A review on the effects of introducing CNTs in the modification process of electrochemical sensors, *Electroanalysis* 31 (2019) 1195.

[23] W. Yang, K. R. Ratinac, S. P. Ringer, P. Thordarson, J. J. Gooding and F. Braet, Carbon nanomaterials in biosensors: should you use nanotubes or graphene? *Angew. Chem. Int. Ed.* 49 (2010) 2114.

[24] P. Britto, K. Santhanam and P. Ajayan, Carbon nanotube electrode for oxidation of dopamine, *Bioelectrochem. Bioenerg.* 41 (1996) 121.

[25] T. R. Madhura, G. G. Kumar and R. Ramaraj, Gold nanoparticles decorated silicate sol-gel matrix embedded reduced graphene oxide and manganese ferrite nanocomposite-materials-modified electrode for glucose sensor application, *J. Chem. Sci.* 131 (2019) 1.

[26] A. Mohammadi, N. Arsalani, A. G. Tabrizi, S. E. Moosavifard, Z. Naqshbandi and L. S. Ghadimi, Engineering rGO-CNT wrapped Co_3S_4 nanocomposites for high-performance asymmetric supercapacitors, *Chem. Eng. J.* 334 (2018) 66.

[27] J. Bai, Y. Li, P. Jin, J. Wang and L. Liu, Facile preparation 3D ZnS nanospheres-reduced graphene oxide composites for enhanced photodegradation of norfloxacin, *J. Alloys Compd.* 729 (2017) 809.

[28] M. Nikzad, M. R. Khanlary and S. Rafiee, Structural, optical and morphological properties of Cu-doped ZnS thin films synthesized by sol–gel method, *Appl. Phys. A* 125 (2019) 1.

[29] L. Kashinath, K. Namratha and K. Byrappa, Sol-gel assisted hydrothermal synthesis and characterization of hybrid ZnS-RGO nanocomposite for efficient photodegradation of dyes, *J. Alloys Compd.* 695 (2017) 799.
[30] B. De Menezes, F. Ferreira, B. Silva, E. Simonetti, T. Bastos, L. Cividanes and G.Thim, Effects of octadecylamine functionalization of carbon nanotubes on dispersion, polarity, and mechanical properties of CNT/HDPE nanocomposites, *J. Mater. Sci.* 53 (2018) 14311.
[31] S. H. Lee, E. Cho, S. H. Jeon and J. R. Youn, Rheological and electrical properties of polypropylene composites containing functionalized multi-walled carbon nanotubes and compatibilizers, *Carbon* 45 (2007) 2810.
[32] S. Pan and X. Liu, ZnS–Graphene nanocomposite: Synthesis, characterization and optical properties, *J. Solid State Chem.* 191 (2012) 51.
[33] M. Sookhakian, Y. Amin, R. Zakaria, W. J. Basirun, M. Mahmoudian, B. Nasiri-Tabrizi, S. Baradaran and M. Azarang, Significantly improved photocurrent response of ZnS-reduced graphene oxide composites, *J. Alloys Compd.* 632 (2015) 201.
[34] X. Chen,H. Li, M. Chen, W. Li, Z. Yuan and R. Snyders, Visible-light-driven photocatalytic activities of monodisperse ZnS-coated reduced graphene oxide nanocomposites, *Mater. Chem. Phys.* 227 (2019) 368.
[35] M. Sharp, M. Petersson and K. Edström, Preliminary determinations of electron transfer kinetics involving ferrocene covalently attached to a platinum surface, *J. Electroanal. Chem. Interf. Electrochem.* 95 (1979) 123.
[36] E. Laviron, General expression of the linear potential sweep voltammogram in the case of diffusionless electrochemical systems, *J. Electroanal. Chem. Interf. Electrochem.* 101 (1979) 19.
[37] A. J. Bard and L. R. Faulkner, *Electrochemical methods: fundamentals and applications* 2nd ed. (Wiley: New York), 2001.
[38] Z. Galus, *Fundamentals of electrochemical analysis* (Ellis Horwood: New York), 1976.
[39] M. Mazloum-Ardakani, H. Mohammadian-Sarcheshmeh, A. Khoshroo and M. Abdollahi-Alibeik, Thiosemicarbazide derivative-functionalized carbon nanotube for simultaneous determination of isoprenaline and piroxicam, *J. Anal. Sci. Technol.* 8 (2017).
[40] 1.J. Wu, T. Zhou, Q. Wang and A. Umar, Morphology and chemical composition dependent synthesis and electrochemical properties of MnO_2-based nanostructures for efficient hydrazine detection, *Sens. Actuator B Chem.* 224 (2016) 878.
[41] F. Xu, Y. Liu, S. Xie and L. Wang, Electrochemical preparation of a three dimensional PEDOT–Cu_xO hybrid for enhanced oxidation and sensitive detection of hydrazine, *Anal. Methods* 8 (2016) 316.
[42] A. A. Ismail, F. A. Harraz , M. Faisal, A. M. El-Toni, A. Al-Hajry and M. Al-Assiri, A sensitive and selective amperometric hydrazine sensor based on mesoporous Au/ZnO nanocomposites, *Mater. Des.* 109 (2016) 530.
[43] M. Sohail, M. Altaf, N. Baig, R. Jamil, M. Sher and A. Fazal, A new water stable zinc metal organic framework as an electrode material for hydrazine sensing, *New J. Chem.* 42 (2018) 12486.
[44] F. Asadi, S. N. Azizi and S. Ghasemi, Preparation of Ag nanoparticles on nano cobalt-based metal organic framework (ZIF-67) as catalyst support for electrochemical determination of hydrazine, *J. Mater. Sci.: Mater. Electron.* 30 (2019) 5410.
[45] Y. Zhang, Y. Zhang, D. Zhang, S. Li, C. Jiang and Y. Su, Confinement preparation of Au nanoparticles embedded in ZIF-67-derived N-doped porous carbon for high-performance detection of hydrazine in liquid/gas phase, *Sens. Actuator B Chem.* 285 (2019) 607.
[46] J. Zhang, H. Liu, M. Dou, F. Wang, J. Liu, Z. Li and J. Ji, Synthesis and characterization of Co_3O_4/multiwalled carbon nanotubes nanocomposite for amperometric sensing of hydrazine, *Electroanalysis* 27 (2015) 1188.
[47] E. Saeb and K. Asadpour-Zeynali, Facile synthesis of TiO_2@ PANI@ Au nanocomposite as an electrochemical sensor for determination of hydrazine, *Microchem. J.* 160 (2021) 105603.
[48] M. Mazloum-Ardakani, Z. Alizadeh, L. Hosseinzadeh, B.B. F. Mirjalili and N. Salehi, An electrochemical based on functionalized carbon nanotube with pyrazole derivative for determination of HZ, *IJAC*, 6 (2019) 49-56.

بررسی رفتار الکتروشیمی بنزوزانتن در الکترود کربن شیشه‌ای اصلاح‌شده با ذرات روی سولفید پیچیده در نانو صفحات گرافن اکسید کاهش یافته/نانولوله کربنی برای اندازه‌گیری هیدرازین

محمد مظلوم اردکانی*، فاطمه جوکار، حمیده محمدیان سرچشمه، بی بی فاطمه میرجلیلی، سحرسادات حسینی خواه

گروه شیمی، دانشکده علوم، دانشگاه یزد، یزد، ایران

تاریخ دریافت: ۳ شهریور ۱۴۰۰ تاریخ پذیرش: ۱ مهر ۱۴۰۰

چکیده

حسگرهای الکتروشیمیایی به علت مزایایی که در مقایسه با روش‌های پرهزینه و پیچیده‌ی دستگاهی دارند مورد توجه وسیعی قرار گرفته‌اند و کاربرد آن‌ها در حوزه‌های مختلف رشد روزافزونی داشته است. در این تحقیق رفتار الکتروشیمیایی الکترود کربن شیشه‌ای اصلاح شده با اصلاحگر و کامپوزیت سه‌تایی شامل صفحات گرافن اکسید کاهش یافته، نانولوله‌های کربنی و ذرات روی سولفید برای اندازه‌گیری هیدرازین بررسی شد. پارامترهایی از اصلاحگر تثبیت شده روی سطح الکترود مانند ضریب انتقال و تعداد الکترون و پروتون مبادله شده در اثر اکسایش، با استفاده از ولتامتری چرخه‌ای مورد بررسی قرار گرفت. از روی نمودار تافل مقدار ضریب انتقال برای هیدرازین ۰,۳۸ تعیین شد. بر مبنای داده های حاصل از کرونوآمپرومتری نیز ضریب نفوذ هیدرازین، برابر $۱,۹۹\times۱۰^{-۵}$ cm^2/s محاسبه شد. همچنین با استفاده از روش ولتامتری ضربانی تفاضلی و رسم نمودن منحنی درجه بندی، ناحیه غلظتی ۰,۸۰–۰,۰۱و ۰,۸۰–۶۰,۰ و حد تشخیص ۰,۰۰۶ میکرو مولار حاصل شد. به منظور بررسی کارایی روش پیشنهادی، اندازه‌گیری در نمونه حقیقی آب شرب انجام گرفت.

واژه‌های کلیدی

روی سولفید؛ گرافن اکسید کاهش یافته؛ حسگر الکتروشیمیایی؛ هیدرازین.